receptor 4 TICAM-1 that induces interferon-beta. J Biol Chem 278:49751–49762
Oshiumi H, Matsumoto M, Hatakeyama S et al (2009) Riplet/RNF135, a RING finger protein, ubiquitinates RIG-I to promote interferon-beta induction during the early phase of viral infection. J Biol Chem 284:807–817
Oshiumi H, Ikeda M, Matsumoto M et al (2010a) Hepatitis C virus core protein abrogates the DDX3 function that enhances IPS-1-mediated IFN-beta induction. PLoS One 5:e14258
Oshiumi H, Sakai K, Matsumoto M et al (2010b) DEAD/H BOX 3 (DDX3) helicase binds the RIG-I adaptor IPS-1 to up-regulate IFN-beta-inducing potential. Eur J Immunol 40:940–948
Oshiumi H, Miyashita M, Inoue N et al (2010c) The ubiquitin ligase Riplet is essential for RIG-I-dependent innate immune responses to RNA virus infection. Cell Host Microbe 8:496–509
Owsianka AM, Patel AH (1999) Hepatitis C virus core protein interacts with a human DEAD box protein DDX3. Virology 257: 330–340
Rathinam VA, Fitzgerald KA (2011) Cytosolic surveillance and antiviral immunity. Curr Opin Virol 1:455–462
Saeed M, Shiina M, Date T et al (2011) In vivo adaptation of hepatitis C virus in chimpanzees for efficient virus production and evasion of apoptosis. Hepatology 54:425–433
Saito T, Owen DM, Jiang F et al (2008) Innate immunity induced by composition-dependent RIG-I recognition of hepatitis C virus RNA. Nature 454:523–527
Sawa Y, Arima Y, Ogura H et al (2009) Hepatic interleukin-7 expression regulates T cell responses. Immunity 30:447–457
Schoggins JW, Wilson SJ, Panis M et al (2011) A diverse range of gene products are effectors of the type I interferon antiviral response. Nature 472:481–485
Schroder M (2009) Human DEAD-box protein 3 has multiple functions in gene regulation and cell cycle control and is a prime target for viral manipulation. Biochem Pharmacol 79: 297–306
Schroder M, Baran M, Bowie AG et al (2008) Viral targeting of DEAD box protein 3 reveals its role in TBK1/IKKepsilon-mediated IRF activation. EMBO J 27:2147–2157
Schulz O, Diebold SS, Chen M et al (2005) Toll-like receptor 3 promotes cross-priming to virus-infected cells. Nature 433: 887–892
Seth RB, Sun L, Ea CK et al (2005) Identification and characterization of MAVS, a mitochondrial antiviral signaling protein that activates NF-kappaB and IRF 3. Cell 122:669–682
Seya T, Matsumoto M (2009) The extrinsic RNA-sensing pathway for adjuvant immunotherapy of cancer. Cancer Immunol Immunother 58:1175–1184
Seya T, Shime H, Takaki H et al (2012) TLR3/TICAM-1 signaling in RIP3 tumor necroptosis. Oncoimmunology 1:917–923
Shimoda S, Harada K, Niiro H et al (2008) Biliary epithelial cells and primary biliary cirrhosis: the role of liver-infiltrating mononuclear cells. Hepatology 47:958–965
Shimoda S, Harada K, Niiro H et al (2011) Interaction between Toll-like receptors and natural killer cells in the destruction of bile ducts in primary biliary cirrhosis. Hepatology 53:1270–1281
Sillanpaa M, Kaukinen P, Melen K et al (2008) Hepatitis C virus proteins interfere with the activation of chemokine gene promoters and downregulate chemokine gene expression. J Gen Virol 89:432–443
Soulat D, Burckstummer T, Westermayer S et al (2008) The DEAD-box helicase DDX3X is a critical component of the TANK-binding kinase 1-dependent innate immune response. EMBO J 27:2135–2146
Takaoka A, Taniguchi T (2008) Cytosolic DNA recognition for triggering innate immune responses. Adv Drug Deliv Rev 60:847–857
Takaoka A, Yanai H, Kondo S et al (2005) Integral role of IRF-5 in the gene induction programme activated by Toll-like receptors. Nature 434:243–249
Tanabe M, Kurita-Taniguchi M, Takeuchi K et al (2003) Mechanism of up-regulation of human Toll-like receptor 3 secondary to infection of measles virus-attenuated strains. Biochem Biophys Res Commun 311:39–48
Thomas E, Gonzalez VD, Li Q et al (2012) HCV infection induces a unique hepatic innate immune response associated with robust production of type III interferons. Gastroenterology 142: 978–988
Uematsu S, Akira S (2007) Toll-like receptors and type I interferons. J Biol Chem 282:15319–15323
Wang N, Liang Y, Devaraj S et al (2009) Toll-like receptor 3 mediates establishment of an antiviral state against hepatitis C virus in hepatoma cells. J Virol 83:9824–9934
Wen C, He X, Ma H et al (2008) Hepatitis C virus infection downregulates the ligands of the activating receptor NKG2D. Cell Mol Immunol 5:475–478
Yeretssian G (2012) Effector functions of NLRs in the intestine: innate sensing, cell death, and disease. Immunol Res 54:25–36
Yoneyama M, Kikuchi M, Natsukawa T et al (2004) The RNA helicase RIG-I has an essential function in double-stranded RNA-induced innate antiviral responses. Nat Immunol 5: 730–737
Yoneyama M, Onomoto K, Fujita T (2008) Cytoplasmic recognition of RNA. Adv Drug Deliv Rev 60:841–846
Zeremski M, Petrovic LM, Talal AH (2007) The role of chemokines as inflammatory mediators in chronic hepatitis C virus infection. J Viral Hepat 14:675–687
Zhang Z, Kim T, Bao M et al (2011) DDX1, DDX21, and DHX36 helicases form a complex with the adaptor molecule TRIF to sense dsRNA in dendritic cells. Immunity 34:866–878
Zhu H, Dong H, Eksioglu E et al (2007) Hepatitis C virus triggers apoptosis of a newly developed hepatoma cell line through antiviral defense system. Gastroenterology 133:1649–1659

THE JOURNAL OF IMMUNOLOGY

Cleaved/Associated TLR3 Represents the Primary Form of the Signaling Receptor

Florent Toscano, Yann Estornes, François Virard, Alejandra Garcia-Cattaneo, Audrey Pierrot, Béatrice Vanbervliet, Marc Bonnin, Michael J. Ciancanelli, Shen-Ying Zhang, Kenji Funami, Tsukasa Seya, Misako Matsumoto, Jean-Jacques Pin, Jean-Laurent Casanova, Toufic Renno and Serge Lebecque

J Immunol 2013; 190:764-773; Prepublished online 19 December 2012;
doi: 10.4049/jimmunol.1202173
http://www.jimmunol.org/content/190/2/764

The Journal of Immunology is published twice each month by
The American Association of Immunologists, Inc.,
9650 Rockville Pike, Bethesda, MD 20814-3994.

Print ISSN: 0022-1767 Online ISSN: 1550-6606.

Cleaved/Associated TLR3 Represents the Primary Form of the Signaling Receptor

Florent Toscano,*,[1] Yann Estornes,*,[1] François Virard,* Alejandra Garcia-Cattaneo,[†] Audrey Pierrot,* Béatrice Vanbervliet,* Marc Bonnin,* Michael J. Ciancanelli,[‡] Shen-Ying Zhang,[‡,§] Kenji Funami,[¶] Tsukasa Seya,[¶] Misako Matsumoto,[¶] Jean-Jacques Pin,[‖] Jean-Laurent Casanova,[‡,§,#] Toufic Renno,* and Serge Lebecque*

TLR3 belongs to the family of intracellular TLRs that recognize nucleic acids. Endolysosomal localization and cleavage of intracellular TLRs play pivotal roles in signaling and represent fail-safe mechanisms to prevent self-nucleic acid recognition. Indeed, cleavage by cathepsins is required for native TLR3 to signal in response to dsRNA. Using novel Abs generated against TLR3, we show that the conserved loop exposed in LRR12 is the single cleavage site that lies between the two dsRNA binding sites required for TLR3 dimerization and signaling. Accordingly, we found that the cleavage does not dissociate the C- and N-terminal fragments, but it generates a very stable "cleaved/associated" TLR3 present in endolysosomes that recognizes dsRNA and signals. Moreover, comparison of wild-type, noncleavable, and C-terminal–only mutants of TLR3 demonstrates that efficient signaling requires cleavage of the LRR12 loop but not dissociation of the fragments. Thus, the proteolytic cleavage of TLR3 appears to fulfill function(s) other than separating the two fragments to generate a functional receptor. *The Journal of Immunology*, **2013, 190: 764–773.**

Toll-like receptors belong to a family of pattern recognition receptors that sense the presence of pathogens and trigger a protective innate immune response (1). These germline-encoded type I integral membrane glycoproteins bind their ligands through their extracellular domain (ECD), which is composed of 19–25 leucine-rich repeats (LRRs) (2). In contrast with other members of the family that primarily recognize molecular patterns specific for nonself invaders, TLR3, TLR7, and TLR9 recognize nucleic acids originating from microbes, as well as from the host. Several fail-safe mechanisms prevent self-polynucleotide recognition and subsequent autoimmune disorders (3). Ligands must be recognized by cell surface receptor(s) (4) that mediate their internalization before encountering the corresponding TLR exclusively in the acidic endolysosomal compartment from which signal transduction can be initiated (5). Delivery of intracellular TLRs to the endocytic compartments is also tightly regulated by the chaperone Unc93b1 (6, 7). Finally, processing by pH-dependent lysosomal proteases is an additional checkpoint for controlling TLR9 activation (8–10).

Although several studies on intracellular TLRs have been based on TLR9 trafficking and processing, less is known about TLR3. TLR3 appears to be dedicated to the recognition of dsRNA (11), and it plays a central role in the defense against HSV-1 infection in the CNS in humans (12–15). Although endogenous mRNA can activate TLR3 in vitro (16), its involvement in the autoimmune response has not been demonstrated. It was shown that TLR3 dimerization is needed for dsRNA binding and signaling (17). Moreover, analysis of the crystal structure (18, 19) and mutagenesis (18, 20, 21) of TLR3 ECD revealed that dsRNA binding requires interaction of the negatively charged ribose backbone of dsRNA with residues of TLR3 dimers located in LRR1 and LRR3, as well as with a second region formed by LRR19–LRR21 that becomes positively charged in the mildly acidified endolysosomal compartment. Therefore, the requirement for cleavage of the ECD for TLR3 signaling (9, 10, 22) raises an intriguing issue with regard to how endogenous TLR3 is processed and which forms of the receptor recognize dsRNA. In this study, we generated and used novel mAbs directed against TLR3 ECD and mutant forms of TLR3 to demonstrate that cleavage of the LRR12 loop, but not separation of the two fragments, is required for signaling.

Materials and Methods

Cell culture and reagents

HEK293 and HEK293-TLR3-hemagglutinin (HA) cells (InvivoGen) were grown in DMEM medium (Invitrogen) supplemented with 10% FBS and penicillin/streptomycin. Human bronchial epithelial cell line BEAS-2B (Sigma) was cultured in LHC-9 medium (Invitrogen) in bovine collagen

*Centre de Recherche en Cancérologie de Lyon, INSERM Unité Mixte de Recherche 1052/Centre National de la Recherche Scientifique 5286, Centre Léon Bérard, 69008 Lyon, France; [†]Institut Curie, INSERM U932, 75005 Paris, France; [‡]St. Giles Laboratory of Human Genetics of Infectious Diseases, Rockefeller Branch, The Rockefeller University, New York, NY 10065; [§]Laboratory of Human Genetics of Infectious Diseases, Necker Branch, INSERM U980, University Paris Descartes, Paris 75015, France; [¶]Department of Microbiology and Immunology, Graduate School of Medicine, Hokkaido University, Kita-ku, Sapporo 060-8638, Japan; [‖]DENDRITICS SAS, Bioparc Laennec, 69008 Lyon, France; and [#]Pediatric Immunology-Hematology Unit, Necker Hospital for Sick Children, Paris 75015, France

[1]F.T. and Y.E. contributed equally to this work.

Received for publication August 21, 2012. Accepted for publication November 15, 2012.

This work was supported by Cancéropôle Lyon-Auvergne-Rhône-Alpes.

F.T., Y.E., F.V., A.G.-C., M.J.C., S.-Y.Z., T.S., M.M., T.R., and S.L. designed the experiments. F.T., Y.E., F.V., A.G.-C., A.P., B.V., S.-Y.Z., M.J.C., M.B., K.F., and J.-J.P. performed experiments and analyzed data. F.T., Y.E., F.V., J.-L.C., T.R., and S.L. wrote the manuscript, with all authors providing detailed comments and suggestions. S.L. directed the project.

Address correspondence and reprint requests to Prof. Serge Lebecque, Centre de Recherche en Cancérologie de Lyon, INSERM Unité Mixte de Recherche 1052/Centre National de la Recherche Scientifique 5286, Centre Léon Bérard, 28 rue Laennec, 69008 Lyon, France. E-mail address: serge.lebecque@univ-lyon1.fr

The online version of this article contains supplemental material.

Abbreviations used in this article: DC, dendritic cell; ECD, extracellular domain; EEA, early endosome Ag; EndoH, endoglycosidase H; ER, endoplasmic reticulum; FL, full length; HA, hemagglutinin; HMW, high molecular weight; LMW, low molecular weight; LRR, leucine-rich repeat; mDC, monocyte-derived dendritic cell; NSCLC, non-small cell lung cancer; PNGase, peptide:*N*-glycosidase F; Poly(A:U), polyadenylic-polyuridylic acid; Poly(I:C), polyinosinic-polycytidylic acid; siRNA, small interfering RNA; WT, wild-type.

www.jimmunol.org/cgi/doi/10.4049/jimmunol.1202173

type I (Invitrogen) and fibronectin (Sigma)-coated dishes. $CD14^+$ monocytes were purified from peripheral blood of healthy donors: PBMCs were isolated from human peripheral blood by standard density-gradient centrifugation on Pancoll (PAN Biotech) and then mononuclear cells were separated from PBLs on a 50% Percoll solution (GE Healthcare). Monocytes were enriched by one step of adherence and differentiated in immature dendritic cells (DCs) in complete RPMI 1640 medium supplemented with 200 ng/ml human GM-CSF (kind gift of Schering-Plough) and 50 ng/ml human rIL-4 (R&D Systems) for 6 d. NCI-H292 and NCI-H1703 non-small cell lung cancer (NSCLC) cell lines (American Type Culture Collection) were grown in RPMI 1640 medium (Invitrogen) supplemented with 10% FBS (Sigma), HEPES, NaPy, 100 U/ml penicillin/streptomycin, and 2 mM glutamine. THP1 and U937 cell lines were grown in RPMI 1640 medium (Invitrogen) supplemented with 10% FBS and 100 U/ml penicillin/streptomycin. IFN-α was from Schering-Plough. Z-FA-fmk, chloroquine, tunicamycin, and cycloheximide were from Sigma. Polyinosinic-polycytidylic acid [Poly(I:C)]-high molecular weight (HMW) and Poly(I:C)-low molecular weight (LMW) were purchased from InvivoGen. polyadenylic-polyuridylic acid [Poly(A:U)] was from Innate Pharma. Mouse monoclonal IgG1 anti-actin Ab was from MP Biomedicals. Anti-mouse TLR3 Ab T3.7C3 was a gift from Nadège Goutagny (Centre de Recherche sur le Cancer de Lyon, Lyon, France). HRP-conjugated donkey anti-mouse secondary Ab was from Jackson ImmunoResearch.

TLR3.2 and TLR3.3 Ab preparation and purification

BALB/C mice were immunized with recombinant human TLR3 ECD (R&D Systems) by three i.p. injections of the immunogen in the presence of Freund's adjuvant and a final i.v. boost, 3 d before spleen isolation. Splenic cells were fused with the SP20 myeloma cell line in the presence of polyethylene glycol. Hybridoma supernatants were screened by immunofluorescent staining of pUNO-hTLR3-HA and pUNO-hTLR3-V5 transiently transfected 293T cells with Exgen 500 (Euromedex) and fixed with acetone. Only clones recognizing both transfected cells were selected.

Western blotting

Cells were lysed in cold lysis buffer (20 mM Tris-HCl [pH 7.4], 150 mM NaCl, 0.2% Nonidet P-40, supplemented with 1 mM orthovanadate, 10 mM NaF, and a protease inhibitor mixture; Sigma) for 25 min on ice. Cell lysates were cleared by centrifugation (13,000 × *g* for 10 min at 4°C), and protein concentration was determined using the Bradford assay (Bio-Rad). Protein lysates were denatured or not in Laemmli buffer containing 1% SDS and 5 mM DTT and heated to 95°C for 5 min. For peptide:*N*-glycosidase F (PNGase)/endoglycosidase H (EndoH) digestions, lysates were treated as recommended by the manufacturer (New England BioLabs). Proteins were resolved on SDS-polyacrylamide gels and transferred onto polyvinylidene difluoride membranes by electroblotting, and nonspecific binding sites were blocked using TBS containing 0.1% Tween-20 and 5% (w/v) dry milk. After incubation with the appropriate secondary Abs conjugated to HRP, blots were revealed using ECL (GE Healthcare) or SuperSignal (Thermo Scientific) reagents. For reimmunoprecipitation experiments, anti-TLR3 or anti-HA immunoprecipitates were eluted with preheated lysis buffer containing 1% SDS and 5 mM DTT; 20% of each sample was resolved by SDS-PAGE, and the remaining 80% was diluted 10-fold in lysis buffer and then reimmunoprecipitated with TLR3.2 or anti-HA Ab, resolved by SDS-PAGE, and analyzed with either TLR3.2 or TLR3.3 Ab.

Immunofluorescence

Cells were washed with PBS, fixed with 4% formaldehyde for 10 min at room temperature, and washed three times with PBS. Cells were then blocked using Image-iT FX signal enhancer (Life Technologies) for 30 min at room temperature and washed once with PBS. Thereafter, each washing step was done using TBS. Cells were incubated for 1 h at room temperature with TLR3.1, anti-HA, anti-calreticulin, early endosome Ag (EEA)1, or Lamp1 (Abcam) primary Abs. After washing three times, cells were incubated for 30 min at room temperature with secondary Abs (goat anti-mouse–Alexa Fluor 488 and goat anti-rabbit–Alexa Fluor 555 or Alexa Fluor 633; Life Technologies). Cells were washed again 3 min each. Cover slips were air-dried and then mounted using ProLong Gold antifade reagent with DAPI (Life Technologies). Images were acquired using a confocal microscope (Zeiss Axiovert 100 M LSM510) with a 1.4 NA Plan-Apochromat 63× oil-immersion lens. Image noise was reduced using a Despeckle Fiji filter.

Cytokines measurement

The supernatant from NCI-H292 and NCI-H1703 cells, cultured or not with 100 μg/ml Poly(I:C) for 24 h, was assayed for IL-6, IP-10, and RANTES using a MILLIPLEX MAP kit (Millipore) on a Luminex Bio-Plex 200 System Analyzer (Bio-Rad). The supernatant from monocyte-derived DCs (mDCs), cultured or not with 100 μg/ml Poly(I:C) for 24 h, was assayed for IL-6, IP-10, TNF-α, and IFN-λ using a Quantikine ELISA test (R&D Systems), as described by the manufacturer.

DNA cloning

Preparation of the LRR1-11 and 13-21 deletion mutants was described previously (23). For the TLR3-Ins12-HA mutant, mutagenesis was performed using the QuikChange XL Site-Directed Mutagenesis Kit (Stratagene) and primer pairs containing deletion of 24 nucleotides: 5′-CTGAATTTGAAACG-GTCTTTTACTCTCCCCAAGATTGATGATTTTTCT-3′ (forward) and 5′-AGAAAAATCATCAATCTTGGGGAGAGTAAAAGACCGTTTCAAA-TTCAG-3′ (reverse). Ten nanograms of plasmid DNA and 125 ng of primers were used, according to the manufacturer's instructions. Two colonies from each library were sequenced.

For the TLR3-$Cter_{356}$-HA mutant, LRR deletion mutants of TLR3 (A_{22}–K_{356}) were generated by PCR with Phusion (Finnzyme), using the appropriate primers: 5′-TGTTTGGAGCACCTTAACATGGAAG-3′ (forward) and 5′-GGTGGAGGATGCACACAGCATCCCA-3′ (reverse). PCR was performed with the following cycling conditions: 10 s at 98°C, 2 min at 72°C for 25 cycles. The PCR product was treated with DpnI to digest the template DNA, phosphorylated with T4 PNK (New England BioLabs), and ligated using a DNA Ligation kit (New England BioLabs). Deletion constructs were sequenced. TLR3-$Cter_{346}$ was provided by P. Bénaroch (Curie Institute, Paris, France).

RNA interference

Synthetic TRIF (L-012833-00-0005) and control nonsilencing (D-001810-03-20) small interfering RNAs (siRNAs) were from Dharmacon. TLR3 Stealth RNAi siRNA (TLR3HSS110816) was from Invitrogen. siRNAs mix was prepared in Opti-MEM medium (Invitrogen), and cells in suspension were transfected using HiPerFect reagent (QIAGEN), as described by the manufacturer. The final siRNA concentrations were 25 nM. Transfected cells were seeded in 6-well plates or 96-well white plates (Greiner) and incubated for 24 h. Medium was replaced with fresh complete medium, and cells were incubated for 48 h before Poly(I:C) treatment.

Generation of ISRE– and NF-κB–luciferase reporter cell lines

HEK293, NCI-H292, and NCI-H1703 cells were transduced with luciferase ISRE- or NF-κB–reporter lentiviruses (SABiosciences), according to the manufacturer's recommendations, and transduced cells were selected with puromycin.

Reporter luciferase assays

Cells were seeded in white 96-well plates (10,000 cells/well); 24 h later they were treated with 10 μg/ml poly(I:C) in 50 μl medium for 4 or 6 h, depending on the cell line. Then, 50 μl Steady-Glo reactive (Promega) was added to each well before reading luminescence with a Tecan Infinite 200 microplate reader using i-control software (Tecan).

Transient expression in HEK293 cells

Cells were seeded in 100-mm dishes to reach ~70% confluence on the day of transfection. Cells were transfected with pUNO, TLR3–wild-type (WT)-HA, TLR3-Ins12-HA, TLR3-$Cter_{356}$-HA, or TLR3-$Cter_{346}$-HA by incubating 8 μl Lipofectamine 2000 (Invitrogen) with 8 μg plasmid in 6 ml Opti-MEM medium for 5 h; subsequently, Opti-MEM was replaced by fresh medium. Twenty-four hours after transfection, cells were trypsinized and seeded in 96-well white plates and 6-well plates and incubated for 24 h.

Stable transfections

P2.1 cells were transfected with pUNO-hTLR3 vectors, which contain WT TLR3 cDNA, TLR3-Ins12 mutant, or TLR3-Cter356 mutant cDNA, or with an empty mock vector, in the presence of Lipofectamine Reagent (Invitrogen) and PLUS Reagent (Invitrogen), as described by the manufacturer. Stable transfectants were selected with medium containing blasticidin (5 μg/ml; Invitrogen). The presence of TLR3 was confirmed by Western blotting.

Determination of mRNA levels by RT-quantitative PCR

Total RNA was extracted from P2.1 cells. RNA was reverse-transcribed using Oligo-deoxy-thymidine. To determine mRNA levels for IL-29, quantitative PCR was performed with Assays-on-Demand probe/primer combinations and 2× universal reaction mixture in an ABI Prism 7700 Sequence Detection System (all from Applied Biosystems). The β-glucuronidase (GUS) gene was used for normalization. Results are expressed according to the ΔCt method, as described by the manufacturer.

Coimmunoprecipitation

Cells were cultured in 150-mm dishes, collected, washed in PBS, and lysed in 750 μl cold lysis buffer (20 mM Tris-HCl [pH 7.4], 150 mM NaCl, 0.2% Nonidet P-40, supplemented with 1 mM orthovanadate, 10 mM NaF, and a protease inhibitor mixture; Sigma) for 25 min on ice. Cell lysates were cleared by centrifugation (13,000 × *g* for 10 min at 4°C). Lysates were precleared with 50 μl Sepharose-6B (Sigma) for 1 h at 4°C and then immunoprecipitated overnight at 4°C with 5 μg mouse anti-TLR3.2, anti-TLR3.3, or control IgG1 Ab (R&D Systems) and the following day in the presence of 20 μl protein G–Sepharose for 3 h at 4°C. Beads were recovered by centrifugation, and immunoprecipitates were washed extensively with lysis buffer and eluted with Laemmli buffer containing 1% SDS and 5 mM DTT and heated to 95°C for 10 min.

TLR3 ECD modeling

The MacPyMOL software (DeLano Scientific) was used to generate the 3D representation of the TLR3 structure shown on Figs. 1C and 5A (PDB:1ZIW).

Statistical analysis

Statistical significance was determined using the Student *t* test.

Results

Profiling endogenous TLR3 expression

To analyze the biology of endogenous TLR3, we generated three new mAbs (designated as TLR3.1, TLR3.2, and TLR3.3) raised against the ECD of the receptor. First, the Abs were validated using HEK293 cells stably expressing TLR3 tagged with a C-terminal HA epitope (HEK293-TLR3-HA). In this model, Western blots probed with anti-HA, TLR3.2, and TLR3.3 Abs revealed an ~130 kDa band corresponding to the expected molecular mass of highly glycosylated TLR3 (Fig. 1A) (24). The stronger signal observed with TLR3.2 suggested that this Ab has a higher affinity for TLR3 than does TLR3.3. In addition, anti-HA and TLR3.2 Abs stained a second band at ~72 kDa similar to the C-terminal fragment of TLR3 observed after cleavage by cathepsin. In addition, TLR3.3 Ab detected a third band (Fig. 1A) not recognized by anti-HA mAb and with a size ~60 kDa that could represent the N-terminal fragment of cleaved TLR3. TLR3.1 Ab did not detect TLR3 by Western blot, but it showed the same staining by immunofluorescence as observed with anti-HA Ab (Fig. 1B, Supplemental Fig. 1A). To unequivocally identify the different bands revealed by TLR3.2 and TLR3.3 Abs on Western blot, we mapped the recognized epitopes using 20 single LRR-deleted forms of the ECD of TLR3 (LRR1–11 and LRR13–21) (23). Fig. 1C establishes that TLR3.2 Ab recognizes an epitope present in LRR20, whereas TLR3.3 binds to an epitope formed by residues present in LRR7 and LRR8. We next verified whether similar expression profiles could be observed in human cells of different origins and wondered how treatment with IFN-α, which is known to upregulate the expression of TLR3 (25), would modify this pattern. We determined TLR3 expression by immunoblot of lysates from mDCs (Fig. 1D), from human monocytic cell lines U937 and THP1 (Supplemental Fig. 1B, 1C), and from human bronchial epithelial cells transformed by SV40-T Ag (BEAS-2B; Supplemental Fig. 1D) or derived from NSCLC (NCI-H292 and NCI-H1703; Fig. 1E). The three forms of TLR3 (130, 72, and 60 kDa) were present in every lysate with the exception of THP1, which did not appear to express TLR3 (Supplemental Fig. 1B) or respond to Poly(I:C) (Supplemental Fig. 1E). Resting MRC-5 cells were also devoid of TLR3, but kinetic analysis showed that IFN-α treatment led first to the detection of the high molecular mass bands (~130 and ~135 kDa) of TLR3, followed by an increase in the intensity of the lower ~72-kDa molecular mass band detected by TLR3.2 mAb (Fig. 1F), suggesting that the former might

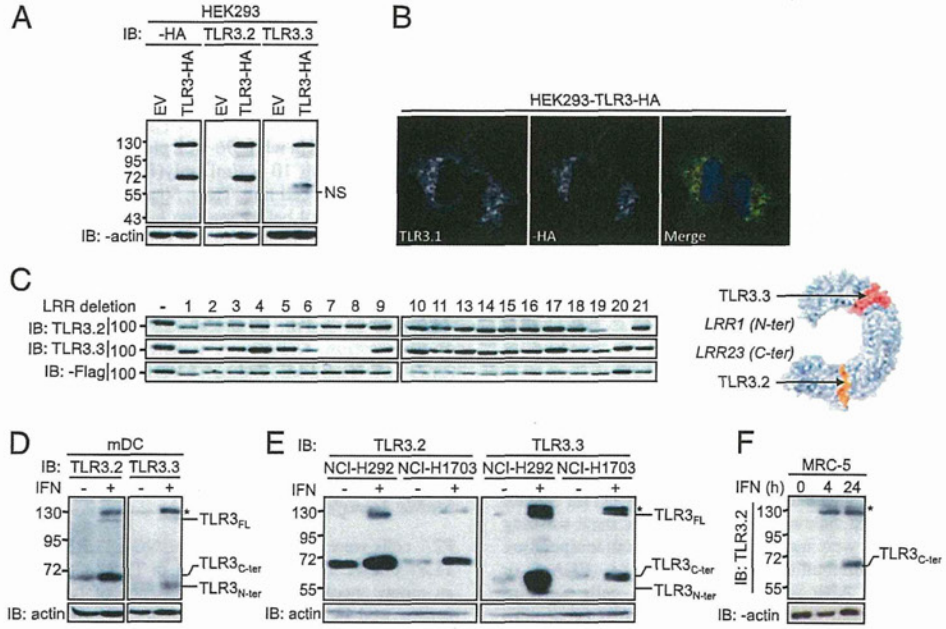

FIGURE 1. Profiling endogenous TLR3 expression. (**A**) Immunoblot analysis of HEK293 cells stably expressing an empty vector (EV) or TLR3-HA; lysates were analyzed with monoclonal anti-HA, TLR3.2, TLR3.3, and anti-actin Abs. (**B**) Immunofluorescence of HEK293 cells stably expressing TLR3-HA; cells were stained with anti-HA or TLR3.1 Abs, followed by DAPI nuclear staining (blue). Original magnification ×63. (**C**) *Left panel*, Epitope mapping of TLR3.2 and TLR3.3 Abs on HEK293 cells stably transfected with TLR3-HA WT (−) or TLR3-HA mutants carrying LRR deletions (1–11 and 13–21, as indicated). Lysates were analyzed with monoclonal TLR3.2, TLR3.3, and anti-Flag Abs, as indicated. *Right panel*, Schematic representation of epitopes recognized by TLR3.2 and TLR3.3 Abs on TLR3 ECD. (**D**) Immunoblot analysis of mDCs treated (+) or not (−) for 18 h with IFN-α (1000 IU/ml); lysates were analyzed with TLR3.2, TLR3.3, and anti-actin Abs. (**E**) Immunoblot analysis of NCI-H292 and NCI-H1703 cells treated (+) or not (−) for 18 h with IFN-α (1000 IU/ml); lysates were analyzed with TLR3.2, TLR3.3, and anti-actin Abs. (**F**) Immunoblot analysis of MRC-5 cells treated (+) or not (−) for the indicated times with IFN-α (1000 IU/ml); lysates were analyzed with TLR3.2 and anti-actin Abs. Values in (A) and (C)–(F) represent molecular mass (kDa). All data are representative of at least three independent experiments. NS, Nonspecific band.

represent the precursors of the latter. In other cell lines, the absolute and relative intensities of the three bands varied depending on the origin of the cells, the Ab used, and the treatment with IFN-α. However, under basal conditions, all cells primarily expressed the 72 and 60 kDa TLR3 forms. Treatment with IFN-α increased the intensity of the three bands and allowed the detection of a higher molecular mass form ~135 kDa in mDCs and in the four cell lines analyzed (asterisk in Fig. 1D–F and Supplemental Fig. 1D). In conclusion, our data suggest that human TLR3 is spontaneously cleaved into a C-terminal fragment ~72 kDa recognized by TLR3.2 and a C-terminal fragment ~60 kDa recognized by TLR3.3, and the relative abundance of cleaved versus uncleaved TLR3 appears to vary with the cell under consideration.

TLR3 ECD cleavage by cathepsins generates two remarkably stable fragments

To further explore the processing of endogenous TLR3 and its functional consequences, we selected the NCI-H292 and NCI-H1703 NSCLC cell lines, which triggered an innate immune response when stimulated with Poly(I:C), as indicated by cytokine secretion (Supplemental Fig. 2A) and by activation of ISRE-dependent luciferase reporter genes (Supplemental Fig. 2B). We ascertained that this response was mediated exclusively by TLR3 by showing its strict dependence on TRIF, the only known adaptor for TLR3 (Supplemental Fig. 2B). We started analyzing the effects of the cathepsin inhibitor Z-FA-fmk on the expression of the different forms of TLR3. Following Z-FA-fmk treatment, the 130 kDa band became more intense with time, whereas the 72 and 60 kDa bands gradually disappeared in both NCI-H292 and NCI-H1703 cells (Fig. 2A, Supplemental Fig. 2C, respectively), as well as in HEK293-TLR3-HA cells (Fig. 2B). These results confirm that cathepsins are necessary for TLR3 cleavage in epithelial cells (22). In NCI-H292 cells, the accumulation of full-length TLR3 was observed as early as 120 min after the addition of Z-FA-fmk (Fig. 2C), whereas in the three cell lines both C-terminal ($TLR3_{C\text{-}ter}$) and N-terminal ($TLR3_{N\text{-}ter}$) TLR3 fragments disappeared with an apparent $t_{1/2}$ >24 h (Fig. 2A, 2B, Supplemental Fig. 2C). Of note, Z-FA-fmk induces a shift of TLR3 full-length ($TLR3_{FL}$) from 130 kDa to 135 kDa ($TLR3_{FL+}$) in both NSCLC cell lines, which is more visible after prolonged gel migration (Fig. 2D). This $TLR3_{FL+}$ could represent the fully glycosylated form of TLR3 leaving the post-Golgi cisternae and not cleaved yet. Published data with regard to the effects of cathepsin inhibitors on TLR3 signaling seem contradictory (8, 9). In this study, we observed that ISRE- and NF-κB–dependent responses to Poly(I:C) were not modified after prolonged treatment with Z-FA-fmk in NCI-H292 cells (Supplemental Fig. 2D), whereas they were significantly, but not completely, suppressed in NCI-H1703 cells (Supplemental Fig. 2E). However, considering the much higher level of TLR3 expression in resting NCI-H292 cells than in NCI-H1703 cells (Fig. 1E), the amounts of $TLR3_{C\text{-}ter}$ detected in NCI-H292 cells after 72 h of treatment with Z-FA-fmk was still comparable to the basal level in NCI-H1703 cells. Therefore, these results suggest that cleaved TLR3 is important for signaling, although uncleaved TLR3 might still transduce some signal. Importantly, Z-FA-fmk treatment blocked TLR3 cleavage and Poly(I:C)-induced cytokine secretion in mDCs (Fig. 2E, 2F) and TR3 signaling in macrophages U937 cells (Fig. 2G, Supplemental Fig. 2F), whereas the response to TNF-α was unaffected. Like with Z-FA-fmk treatment, exposure to the lysosomotropic weak base chloroquine, which prevents cathepsin activity, led to the accumulation of $TLR3_{FL+}$ within 3 h and to the reciprocal disappearance of the two TLR3 fragments in NCI-H292 (Fig. 2H) and NCI-H1703 (Supplemental Fig. 2G) cells after 48 h. The same results were obtained with the specific inhibitor of vacuolar H^+ ATPase Bafilomycin (data not shown). Furthermore, short-term blockade of de novo protein synthesis with cycloheximide confirmed the relative high stability of endogenous $TLR3_{C\text{-}ter}$ (apparent $t_{1/2}$ > 24 h) (Fig. 2I, 2J) compared with $TLR3_{FL}$ (apparent $t_{1/2}$ < 4 h). Despite a weaker signal, a half-life similar to $TLR3_{C\text{-}ter}$ was estimated for $TLR3_{N\text{-}ter}$ (Fig. 2H, Supplemental Fig. 2G). Altogether, our data indicate that, in resting cells, TLR3 is actively transcribed and rapidly cleaved by cathepsins upon its transfer in endolysosomes into two highly stable proteolytic fragments, in agreement with a very recent report (26).

TLR3 transits steadily through the Golgi before being cleaved in the endolysosomal compartments

Although TLR3, like other intracellular TLRs, depends on the chaperone protein Unc93b1 for proper trafficking, it is unclear whether its transfer to the endolysosomes occurs constitutively or in response to its ligand. Using TLR3.1 Ab, we observed by immunofluorescence microscopy that TLR3 colocalizes extensively with Lamp1 (a lysosome marker) but not with EEA1 (an early endosome marker) (Fig. 3A, Supplemental Fig. 3) in resting epithelial cells and that the level of colocalization remained unchanged after stimulation with dsRNA (Supplemental Fig. 3). We next addressed the trafficking of TLR3 by analyzing the N-glycosylation status of the protein, which represents ~35% of its total mass (24). After treatments of cell lysates with PNGase, which removes all N-glycans, $TLR3_{FL}$ and $TLR3_{FL+}$ shifted from 130 and 135 kDa, respectively, to 95 kDa (Fig. 3B, 3C), corresponding to the expected molecular mass of nonglycosylated neosynthesized $TLR3_{FL}$ (904 aa). The $TLR3_{C\text{-}ter}$ band shifted from 72 to 50 kDa, indicating that both cleaved and noncleaved TLR3 are glycosylated. Treatment with EndoH, an endoglycosidase that cleaves N-glycans before their further modification in the Golgi apparatus, indicates that noncleaved $TLR3_{FL}$ is EndoH sensitive, whereas $TLR3_{FL+}$ and $TLR3_{C\text{-}ter}$ are partially EndoH resistant. This was similar to the presence of hybrid glycans on TLR9 even after trafficking through the Golgi (27). Cell treatment with tunicamycin, a de novo *N*-glycosylation inhibitor, caused the rapid fading of $TLR3_{FL}$ (apparent $t_{1/2}$ < 8 h) and the appearance of a band at ~95 kDa representing neosynthesized nonglycosylated full-length TLR3 (Fig. 3D, 3E). Altogether, our data indicate that $TLR3_{FL}$ corresponds to the small amounts of TLR3 present in the endoplasmic reticulum (ER), which is steadily translocated to the Golgi in resting cells, converted into fully glycosylated $TLR3_{FL+}$, and exported to the endosomes/lysosomes, where it is rapidly cleaved.

The endolysosomal pool of cleaved TLR3 is sufficient for signaling

To determine which forms of endogenous TLR3 are functional, we started using specific siRNA and took advantage of the prolonged stability of cleaved fragments versus $TLR3_{FL}$. We observed that 24 and 48 h after transfection, $TLR3_{FL}$ had completely disappeared, whereas the two cleavage fragments were still abundant (Fig. 4A, Supplemental Fig. 4A). Under these conditions, the Poly(I:C)-induced ISRE-dependent response was not reduced (Fig. 4B), suggesting that the uncleaved $TLR3_{FL}$ does not contribute significantly to downstream signaling, probably because of its weak expression compared with the cleaved fragments from the beginning of the experiment. Indeed, ISRE activation faded away gradually with time as the presence of cleaved TLR3 decreased (Fig. 4A, 4B). Similar results were obtained with a NF-κB–dependent reporter gene (Supplemental Fig. 4B). These data show that cleaved TLR3 can signal in the absence of uncleaved $TLR3_{FL}$ and may even represent the predominant signaling form of the receptor.

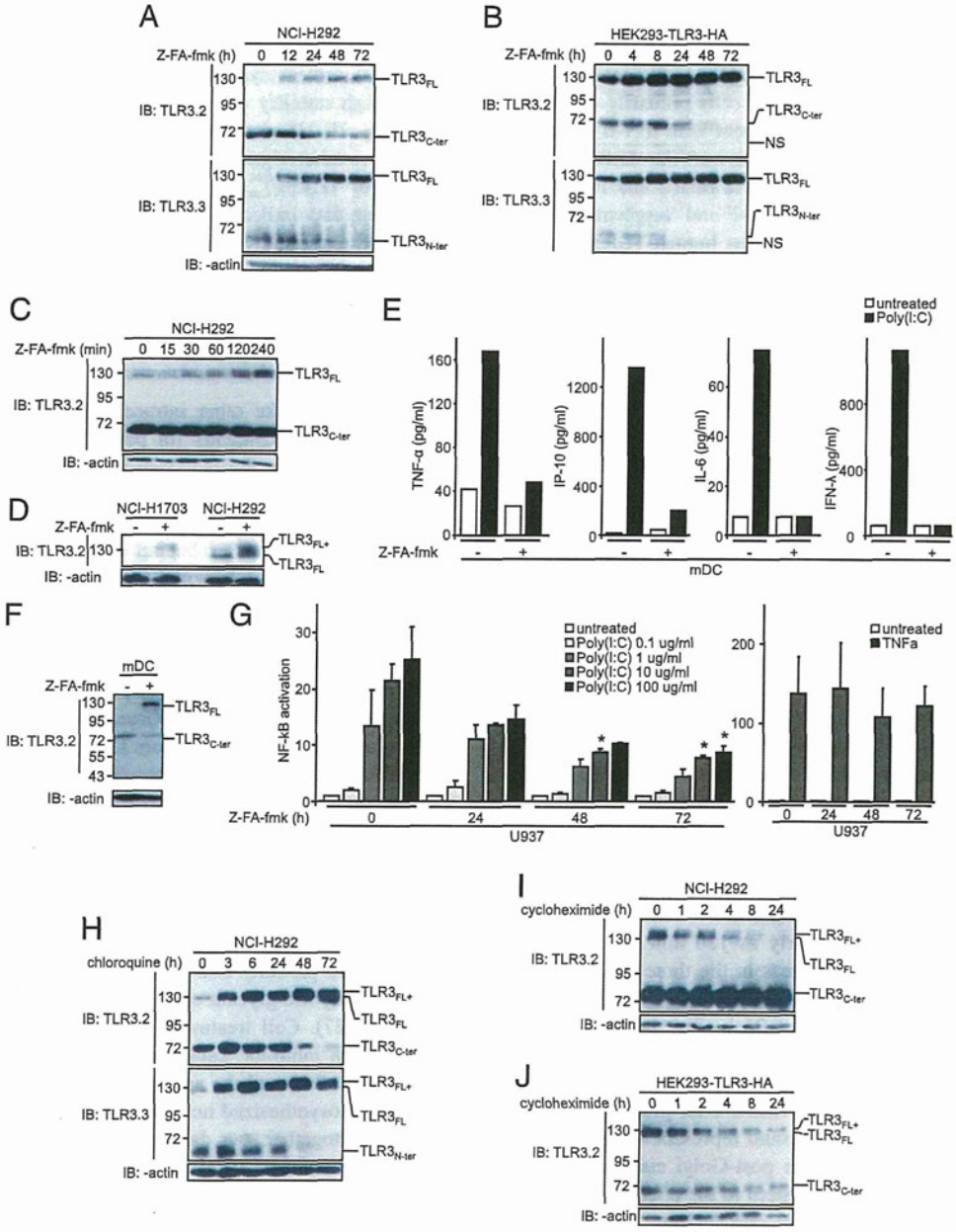

FIGURE 2. Cleavage by cathepsins generates two TLR3 stable fragments. (**A**) Immunoblot analysis of NCI-H292 cells treated for the indicated times with Z-FA-fmk (20 μM) renewed every 24 h. Lysates were analyzed with TLR3.2, TLR3.3, and anti-actin Abs. (**B**) Immunoblot analysis of HEK293-TLR3-HA cells treated for the indicated times with Z-FA-fmk (20 μM) renewed every 24 h. Lysates were analyzed with TLR3.2 and TLR3.3 Abs. (**C**) Immunoblot analysis of NCI-H292 cells treated for the indicated times with Z-FA-fmk (20 μM). Lysates were analyzed with TLR3.2 and anti-actin Abs. (**D**) Immunoblot analysis of NCI-H292 and NCI-H1703 cells treated for 24 h with Z-FA-fmk (20 μM). Lysates were analyzed with TLR3.2 and anti-actin Abs. (**E**) Cytokine production in mDCs that were pretreated for 48 h with Z-FA-fmk and then treated with Poly(I:C) (10 μg/ml) for 24 h. (**F**) Immunoblot analysis of mDCs that were treated or not for 72 h with Z-FA-fmk (20 μM); lysates were analyzed with TLR3.2 and anti-actin Abs. (**G**) NF-κB reporter assay in U937 cells that were pretreated for the indicated times with Z-FA-fmk (20 μM), renewed every 24 h, and then treated with Poly(I:C) at the indicated concentrations (*left panel*) or with TNF-α (50 ng/ml) (*right panel*) for 4 h. (**H**) Immunoblot analysis of NCI-H292 cells treated for the indicated times with chloroquine (1 μg/ml). Lysates were analyzed with TLR3.2, TLR3.3, and anti-actin Abs. (**I**) Immunoblot analysis of NCI-H292 cells treated for the indicated times with cycloheximide (1.5 μg/ml). Lysates were analyzed with TLR3.2 and anti-actin Abs. (**J**) Immunoblot analysis of HEK293-TLR3-HA cells treated for the indicated times with cycloheximide (1.5 μg/ml). Lysates were analyzed with TLR3.2 and anti-actin Abs. Values represent molecular mass (kDa). Data are mean (G) or representative (A–F, H–J) of at least three independent experiments. $*p < 0.05$, untreated cells versus Z-FA-fmk–treated cells.

The N- and C-terminal fragments of TLR3 ECD are needed for efficient signaling

To definitely establish the functionality of uncleaved versus cleaved TLR3, we expressed three mutants of TLR3 in HEK293 cells. Given the apparent molecular mass of deglycosylated $TLR3_{C\text{-}ter}$ and $TLR3_{FL}$ (50 and 95 kDa, respectively; Fig. 3B, 3C), the highly conserved insertion within LRR12, which protrudes on the glycosylation-free side of LRR12 (residues 335–342) (28–31), was a likely site for proteolysis. Thus, the first mutant lacked the entire LRR12 insertion (TLR3-Ins12-HA), whereas the two others represented the C-terminal fragment starting just at the end of the LRR12 insertion (aa 346: TLR3-$Cter_{346}$-HA), as established and

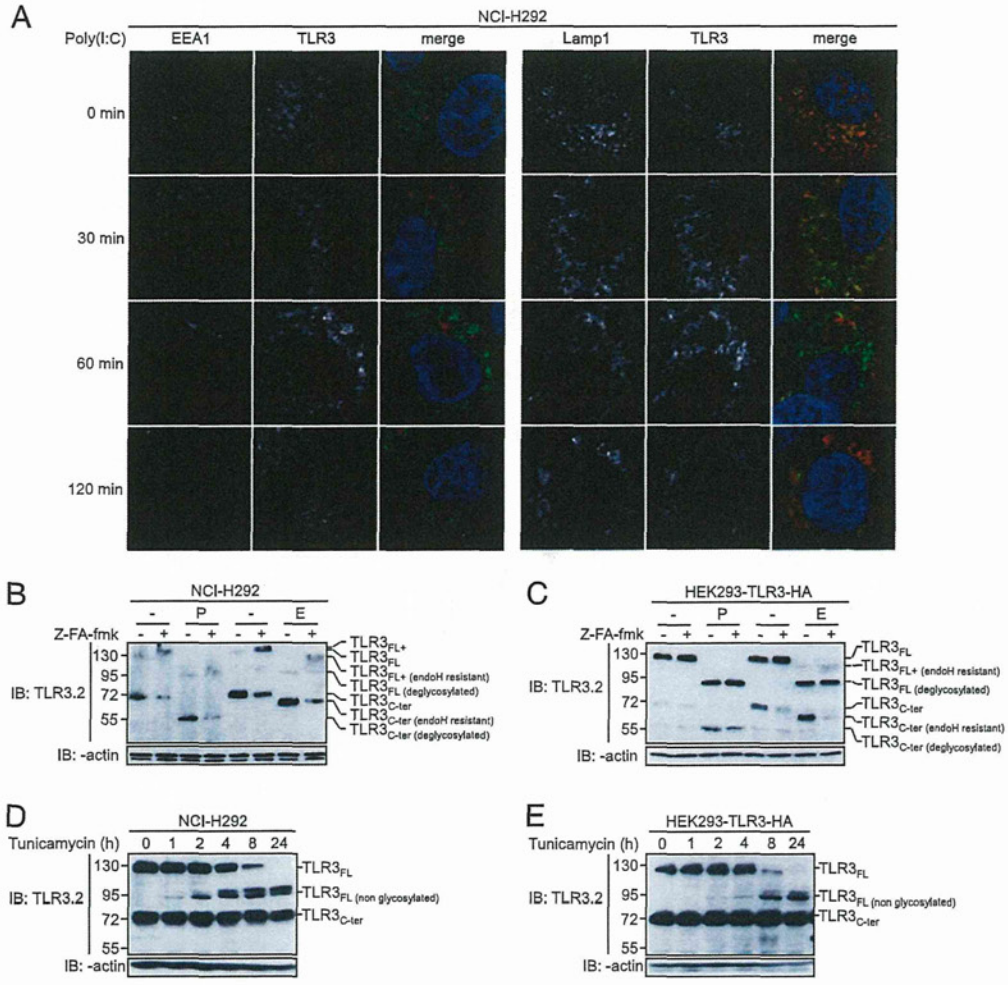

FIGURE 3. TLR3 transits through the Golgi before being cleaved in the endolysosomal compartments. (**A**) Immunofluorescence of NCI-H292 cells treated for the indicated times with Poly(I:C) (10 μg/ml) and then stained with EEA1 or Lamp1, and TLR3.1 Abs, followed by DAPI nuclear staining (blue). Original magnification ×63. (**B**) Immunoblot analysis of NCI-H292 cells that were treated or not with Z-FA-fmk (20 μM) for 24 h. Lysates were left untreated (−) or were treated (+) with PNGase (P) or EndoH (E) and then analyzed with TLR3.2 and anti-actin Abs. (**C**) Immunoblot analysis of HEK293-TLR3-HA cells that were treated or not with Z-FA-fmk (20 μM) for 24 h. Lysates were left untreated (−) or were treated (+) with PNGase (P) or EndoH (E) and then analyzed with TLR3.2 and anti-actin Abs. (**D**) Immunoblot analysis of NCI-H292 cells that were treated for the indicated times with tunicamycin (1 μg/ml). Lysates were analyzed with TLR3.2 and anti-actin Abs. (**E**) Immunoblot analysis of HEK293-TLR3-HA cells that were treated for the indicated times with tunicamycin (1 μg/ml). Lysates were analyzed with TLR3.2 and anti-actin Abs. Values in (B)–(D) represent molecular mass (kDa). Data are representative of at least three independent experiments.

characterized by Garcia-Cattaneo et. al (22), or at the beginning of LRR13 (aa 356: TLR3-Cter$_{356}$-HA) (Fig. 5A). Immunoblots confirmed that all three constructs were expressed at comparable levels in HEK-293T–transfected cells (Fig. 5B), with TLR3-Ins12-HA expressed as a single 130-kDa band, confirming that the LRR12 insertion contains the cleavage site and that TLR3-Ins12-HA is a noncleavable form of the receptor. As expected, lysates from TLR3-Cter$_{356}$-HA– or TLR3-Cter$_{346}$-HA–transfected cells contained a single form ~72 kDa, whose size is consistent with the predicted length of each construct (Fig. 5B). We also observed that treatment with Poly(I:C) did not modify the processing of TLR3 and, particularly, did not induce the cleavage of TLR3-Ins12-HA (Fig. 5B).

When expressed in HEK293 cells, the noncleavable form of the receptor showed the capacity to activate ISRE- and NF-κB–dependent transcription in response to 10 μg/ml of Poly(I:C) (Fig. 5C)

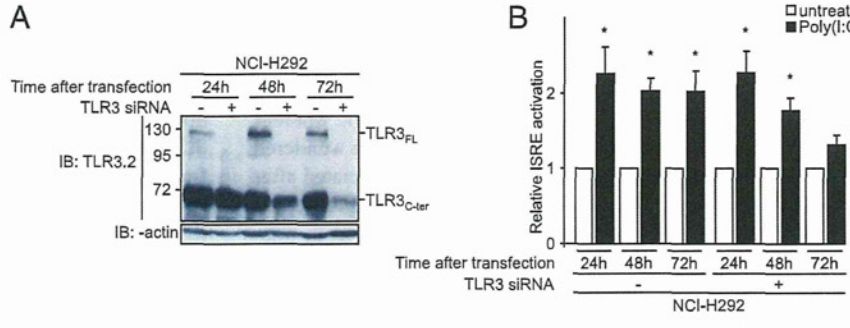

FIGURE 4. Endogenous cleaved TLR3 is sufficient to fully signal. (**A**) Immunoblot analysis of NCI-H292 cells at the indicated times after nonsilencing (−) or TLR3 (+) siRNA transfections (25 μM). Lysates were analyzed with TLR3.2 and anti-actin Abs. (**B**) ISRE reporter assay in NCI-H292 cells at the indicated times after nonsilencing (−) or TLR3 (+) siRNA transfections (25 μM) and treatment without or with Poly(I:C) (10 μg/ml) for 4 h. Data are representative (A) or the mean (B) of three independent experiments. Error bars represent SEM. *$p < 0.05$, untreated cells versus Poly(I:C)-treated cells.

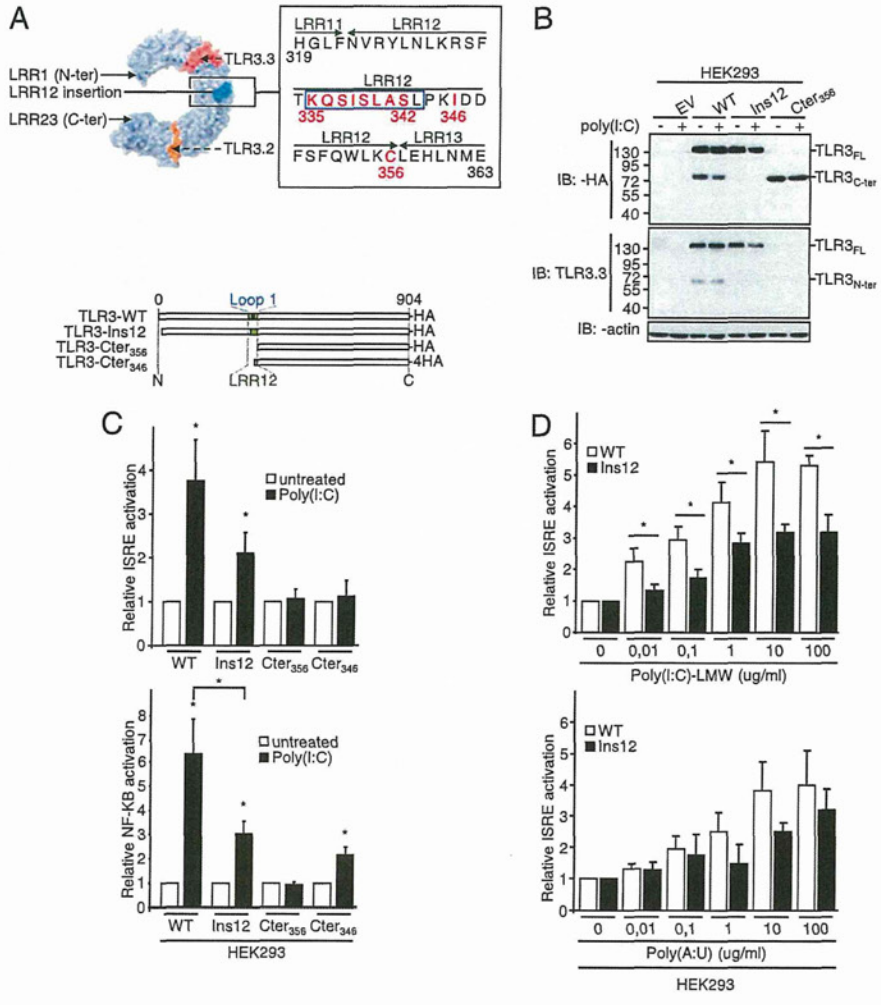

FIGURE 5. Noncleaved TLR3 can signal but the isolated C-terminal TLR3 fragment cannot. (**A**) *Upper panel*, Model of the putative location of the cleavage on LRR12 and TLR3 sequence with starting points of TLR3-Cter$_{356}$ and TLR3-Cter$_{346}$ mutants and deleted sequence (aa 335–342) of TLR3-Ins12 (in red). Blue framework: LRR12 loop1. *Lower panel*, Schematic representation of TLR3 mutants. (**B**) Immunoblot analysis of HEK293 cells transfected with empty vector (EV), TLR3-WT-HA (WT), TLR3-Ins12-HA (Ins12), or TLR3-Cter$_{356}$-HA (Cter$_{356}$) and then treated without (−) or with (+) Poly(I:C) (10 μg/ml) for 4 h. Lysates were analyzed with anti-HA, TLR3.3, and anti-actin Abs. Values represent molecular mass (kDa). (**C**) ISRE (*upper panel*) and NF-KB (*lower panel*) reporter assay in HEK293 cells transfected with TLR3-WT-HA, TLR3-Ins12-HA, TLR3-Cter$_{356}$-HA (Cter$_{356}$), or TLR3-Cter$_{346}$-HA (Cter$_{346}$), and then treated without (white) or with (black) Poly(I:C) (10 μg/ml) for 6 h. (**E**) ISRE reporter assay in HEK293 cells transfected with TLR3-WT-HA or TLR3-Ins12-HA and then treated with the indicated concentrations of Poly(I:C)-LMW or Poly(A:U) for 6 h. Data are representative (B) or the mean (C, D) of at least three independent experiments. Error bars (C, D) represent SEM. *$p < 0.05$, untreated versus Poly(I:C)-treated cells or response of TLR3-WT versus mutant TLR3.

but with significantly reduced efficiency for NF-κB compared with WT TLR3. In contrast, TLR3-Cter$_{356}$-HA was unable to activate either pathway, and TLR3-Cter$_{346}$-HA triggered a weak NF-κB response but no ISRE-dependent response. We next compared the levels of ISRE-dependent transcription in response to increasing concentrations of either LMW Poly(I:C) or Poly(A:U). The dose responses showed that HEK293 cells transfected with WT TLR3 were also significantly more sensitive to LMW Poly(I:C) but not to Poly(A:U) (Fig. 5D). Notably, both C-terminal fragments of the receptor were completely unresponsive to all doses of these two ligands (data not shown). Taken together, these results show that, in agreement with previous reports, uncleaved TLR3 can generate a response to dsRNA (30), whereas the isolated C-terminal fragment triggers only a weak signal (26).

The N- and C-terminal fragments of TLR3 remain associated after cleavage

Because cleaved TLR3 was able to signal in the total absence of TLR3$_{FL}$ (Fig. 4A, 4B, Supplemental Fig. 4A, 4B), whereas isolated TLR3$_{C\text{-}ter}$ was almost ineffective (Fig. 5C), we wondered whether the two fragments of TLR3 could remain associated after proteolytic cleavage. Therefore, we compared the profiles of TLR3 on Western blot performed with lysates prepared in nondenaturing (protein lysate neither reduced nor heated) versus denaturing conditions (Fig. 6A–D, Supplemental Fig. 4C). In nondenaturing conditions, we detected the 130 kDa band, whereas bands corresponding to the proteolytic fragments were barely detectable in epithelial NCI-H292 cells (Fig. 6A, Supplemental Fig. 4C), in mDCs (Fig. 6B), as well as in HEK293-TLR3-HA cells (Fig. 6C, 6D). We ensured that nondenaturing conditions did not prevent the migration of TLR3 fragments, because the constructs corresponding to the cleaved TLR3$_{C\text{-}ter}$ fragment (Cter$_{356}$ and Cter$_{346}$) migrated at expected molecular mass (~72 kDa; Fig. 6D). In contrast, when the same lysates were analyzed in denaturing conditions, TLR3$_{C\text{-}ter}$ and TLR3$_{N\text{-}ter}$ became clearly visible (Fig. 6A–D, Supplemental Fig. 4C), thereby revealing the presence of both uncleaved and cleaved/associated TLR3 in cells. Similarly, when nondenatured lysates were immunoblotted after running on a native gel, the same high molecular band was observed, with HEK293 cells expressing either WT or noncleavable TLR3 and with epithelial cells expressing endogenous TLR3 (Supplemental Fig. 4D). In contrast, the TLR3$_{C\text{-}ter}$ mutant migrated on the same gel at a much lower molecular mass. Moreover, nondenaturing conditions showed that Poly(I:C) treatment did not dissociate TLR3$_{C\text{-}ter}$ and TLR3$_{N\text{-}ter}$ (Fig. 6A–C, Supplemental Fig. 4C). To definitely confirm the association of the two cleaved fragments, we performed immunoprecipitation with C-terminal–specific TLR3.2 and N-terminal–specific TLR3.3 Abs and analyzed the precipitates by immunoblot with the two Abs. In all cases, TLR3$_{N\text{-}ter}$ and TLR3$_{C\text{-}ter}$ coimmunoprecipitated both in NCI-H292 cells (Fig. 6E) and HEK293-TLR3-HA cells (Fig. 6F). Lastly, reprecipitation after denaturation of the immunoprecipitates ob-

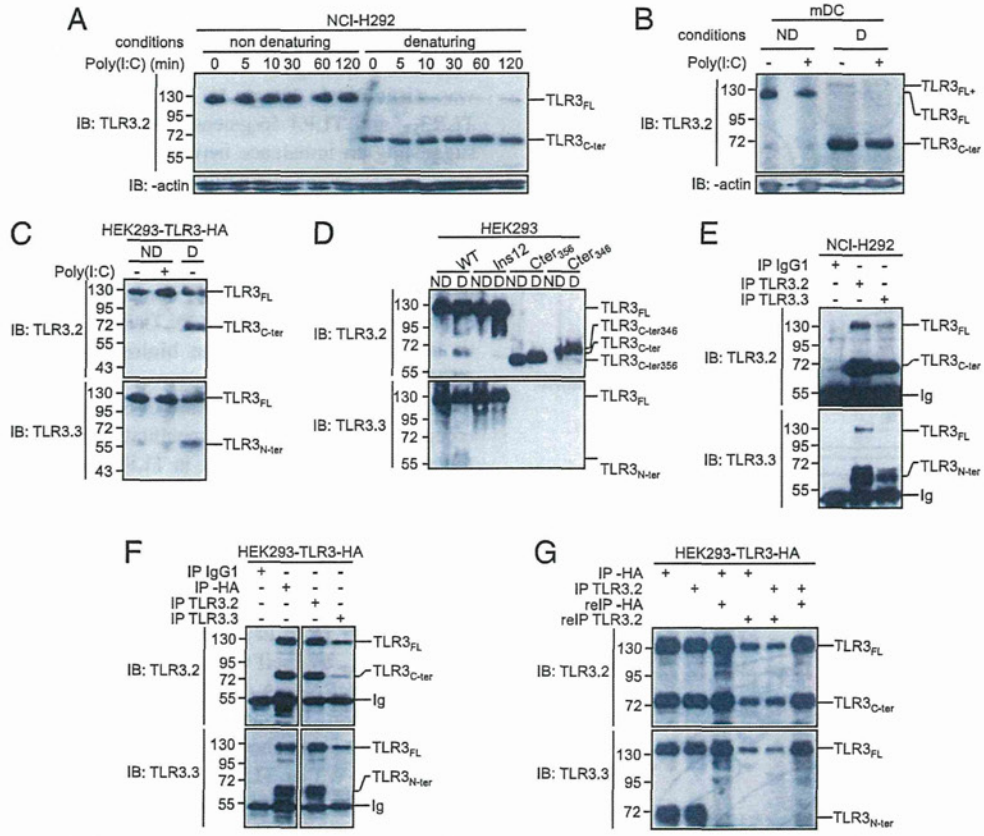

FIGURE 6. The N- and C-terminal fragments of endogenous TLR3 fragments remain associated after cleavage. (**A**) Immunoblot analysis of NCI-H292 cells treated with Poly(I:C) (10 μg/ml) for the indicated times. Lysates were denatured (D) or not (ND) and then analyzed with TLR3.2 and anti-actin Abs. (**B**) Immunoblot analysis of mDCs treated (+) or not (−) with Poly(I:C) (10 μg/ml) for the indicated times. Lysates were denatured (D) or not (ND) and then analyzed with TLR3.2 and anti-actin Abs. (**C**) Immunoblot analysis of HEK293-TLR3-HA cells treated (+) or not (−) with Poly(I:C) (10 μg/ml) for 2 h. Lysates were denatured (D) or not (ND) and then analyzed with TLR3.2 and TLR3.3 Abs. (**D**) Immunoblot analysis of HEK293 cells transfected with TLR3-WT-HA (WT), TLR3-Ins12-HA (Ins12), TLR3-Cter$_{356}$-HA (Cter$_{356}$), or TLR3-Cter$_{346}$-HA (Cter$_{346}$). Lysates were denatured (D) or not (ND) and then analyzed with TLR3.2 and TLR3.3 Abs. (**E**) Immunoblot analysis of NCI-H292 cells. Lysates were immunoprecipitated with IgG1, TLR3.2, or TLR3.3 Abs and analyzed with TLR3.2 and TLR3.3 Abs. (**F**) Immunoblot analysis of HEK293-TLR3-HA cells. Lysates were immunoprecipitated with IgG1, anti-HA, TLR3.2, or TLR3.3 Abs and analyzed with TLR3.2 and TLR3.3 Abs. (**G**) Immunoblot analysis of HEK293-TLR3-HA cells. Lysates were immunoprecipitated with anti-HA or TLR3.2 Abs and then precipitates were reimmunoprecipitated with anti-HA or TLR3.2 Abs and analyzed with TLR3.2 and TLR3.3 Abs. Values represent molecular mass (kDa). Data are representative of at least three independent experiments.

tained with a C-terminal–specific Ab (either TLR3.2 or anti-HA) led to the loss of the N-terminal fragment of TLR3, confirming that the association of the two fragments was through a noncovalent bond (Fig. 6G). Taken together, our data show that the two fragments of TLR3 remain associated after cleavage and that ligand binding does not disrupt this association (Fig. 7). Therefore, the cleaved/associated TLR3 represents the relevant endogenous TLR3 responsible for the majority of immunological functions.

Discussion

Remarkable progress has been made recently in our understanding of the biology of nucleic acid–sensing TLR3, TLR7, and TLR9. Notably, various data now suggest a model in which exogenous nucleotides can be recognized with high sensitivity, whereas self-nucleotide–induced signaling and autoimmunity are prevented (3). Discrimination between nonself- and self-nucleotides appears to be facilitated by several levels of regulation. Recently, cleavage of TLR9 in endolysosomes was shown to be required for generating the C-terminal fragment of the receptor that binds dsDNA with high affinity and signals. Published data indicated that this mechanism might also apply to TLR3 and TLR7 (9, 22). However, our data allow us to propose an alternative model for TLR3 biology (Fig. 7), which reconciles two requisites: the need to restrict dsRNA recognition in endolysosomes (and therefore to expose the receptor to a proteolytic environment) to prevent autoreactivity, as described for other endosomal TLRs, and the requirement of the two ligand binding sites present on the ECD of TLR3—the first near the N terminus and the second close to the transmembrane region—to recognize dsRNA with high avidity. Several aspects of the trafficking and processing of TLR3 diverge from what has been described for other lysosomal TLRs (8, 10).

Building on previous observations, and supported by data that were published after the submission of our manuscript (26), our results allow improvement of our model of TLR3 biology. In contrast to TLR9, which was reported to reside principally in the ER in resting cells (32) and to reach the acidic compartments after stimulation by double-stranded DNA (5–7, 33), TLR3 is continuously exported to the Golgi and accumulates in the endolysosomal compartments where it undergoes a single cleavage by cathepsins, most likely within the short (9 aa) LRR12 external loop; however, the exact cleavage site remains unknown. In contrast, asparagine endopeptidase first cleaves the long (30 aa) LRR14–15 flexible loop of TLR9 that is secondarily trimmed by cathepsins (8–10, 34, 35). Strong conservation of the LRR12 ex-